Available online at www.sciencedirect.com
SCIENCE DIRECT
Polymer 46 (2005) 7094–7108
polymer
www.elsevier.com/locate/polymer

About morphology in ethylene–propylene(-diene) copolymers-based latexes

Delphine L. Tillier[a], Jan Meuldijk[b], Günther W.H. Höhne[c], Peter M. Frederik[d], Oren Regev[e], Cor E. Koning[a,*]

[a]*Laboratory of Polymer Chemistry (SPC), Eindhoven University of Technology, P.O. Box 513, 5600 MB Eindhoven, The Netherlands*
[b]*Process Development Group (SPD), Eindhoven University of Technology, P.O. Box 513, 5600 MB Eindhoven, The Netherlands*
[c]*Department of Polymer Technology (SKT), Eindhoven University of Technology, P.O. Box 513, 5600 MB Eindhoven, The Netherlands*
[d]*Department of Pathology, Electron Microscopy Unit, University of Maastricht, Universiteitssingel 50, 6229 ER Maastricht, The Netherlands*
[e]*Department of Chemical Engineering, The Ilse Katz Center for Meso and Nanoscale Science and Technology, Ben-Gurion University of the Negev, 84105 Beer-Sheva, Israel*

Received 10 December 2004; received in revised form 16 March 2005; accepted 9 May 2005
Available online 23 June 2005

Abstract

Coatings and engineering plastics often require high impact strength. This property can be achieved with tougheners. For the present paper, core-shell impact modifiers were synthesized using ethylene–propylene copolymers (EPM), ethylene–propylene-diene copolymers (EPDM) or a mixture of both types (EP(D)M) as core material, as well as poly(methyl methacrylate) (PMMA) as shell material.

EP(D)M-based polymers were dispersed in water using an Ultra-Turrax® and a high pressure homogenizer. The prepared artificial latexes were used, either without further treatment or after crosslinking, as seed latexes in the emulsion polymerization of methyl methacrylate (MMA). The free radical seeded emulsion polymerization of MMA was investigated in the presence of an oil-soluble initiator, i.e. cumene hydroperoxide (CHP), combined with a redox system, i.e. sodium formaldehyde sulfoxylate hydrate (SFS), disodium salt of ethylenediamine tetra-acetic acid (EDTA), iron (II) sulfate heptahydrate ($FeSO_4$). This initiation system promotes polymerization of MMA near the surface of the seed particles, partially suppressing homogeneous secondary nucleation and polymerization in the aqueous phase.

Kinetic and thermodynamic considerations were used to predict the particle morphology. The monomer type, the monomer-to-rubber ratio, the monomer feed type, and crosslinking of the seed latex particles were investigated, to optimize the polymerization kinetics and the properties of the resulting dispersions. The particle morphology was determined by cryo-transmission electron microscopy (cryo-TEM). Monomer-flooded conditions led to the formation of inverted core-shell particles, whereas starved–feed MMA or MMA/styrene mixtures gave rise to partially engulfed structures, i.e. snowman-like. Crosslinking of the EP(D)M seed particles was found to be required to provide the desired core-shell structures.

Finally, the obtained core-shell structured particles were used to toughen a PMMA matrix. The tensile properties of the modified PMMA matrix were investigated. The micro-morphology of modified PMMA was studied by scanning electron microscopy (SEM). Tensile tests as well as TEM and SEM analyses demonstrated that the main mechanism of deformation operating in the EP(D)M-toughened PMMA matrix is shear yielding, accompanied by debonding and cavitation processes.

Keywords: Impact modifier; Seeded emulsion polymerization of methyl methacrylate (MMA); Morphology

1. Introduction

For many applications, high performance materials, e.g. coatings [1,2] and engineering plastics [3–8], require high impact strength. The paint of a car, for instance, should withstand being hit by a piece of gravel without film rupture. Thermoplastic materials, such as polycarbonate (PC), have a tendency to undergo brittle failure under environmental stress cracking conditions, e.g. by the presence of a sharp notch. Therefore, such materials need some adjustments to extend their applications under high impact conditions, for example in the automotive industry.

* Corresponding author. Tel.: +31 40 247 5353; fax: +31 40 246 3966.
E-mail address: c.e.koning@tue.nl (C.E. Koning).

0032-3861/$ - see front matter © 2005 Elsevier Ltd. All rights reserved.
doi:10.1016/j.polymer.2005.05.095

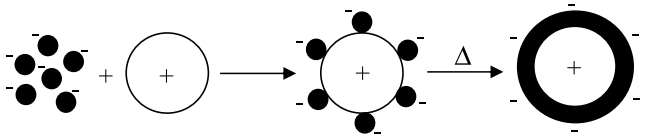

Fig. 1. Preparation of core-shell particles by heterocoagulation [11].

Improvement of impact strength may be achieved with tougheners, which consist of an elastomeric part, providing impact resistance, and a rigid part, providing good adhesion with a polymer matrix. Core-shell tougheners with a crosslinked core, as opposed to linear tougheners, have a fixed morphology and are the preferred impact modifiers, especially in injection molded engineering plastics and in coatings.

The size, volume fraction and morphology of rubber particles dispersed in a polymer matrix are of considerable importance. Emulsion polymerization [9] is usually the method of choice for the preparation of well-defined particles. Excessive heat evolvement and viscosity problems, as encountered during polymerizations in homogeneous media, i.e. bulk or solution polymerization, may be overcome by the use of water as dispersing medium.

Methods of preparation of core-shell polymers include controlled surface precipitation of the coating materials on a core material, or direct surface reactions.

One of the most commonly used precipitation methods is controlled heterocoagulation. Controlled heterocoagulation has been applied, for instance, by Okubo et al. [10] to produce soft core-hard shell composite polymer particles. As depicted in Fig. 1, see Li et al. [11], dispersions of oppositely charged large and small particles are first synthesized. The small particles should exhibit a glass transition temperature lower than the glass transition or melting temperature of the large core particles. When both dispersions are mixed, heterocoagulation occurs driven by electrostatic attraction. This heterocoagulation results in the formation of a monolayer of small beads on the surface of large cores. After controlled heat processing, a homogeneous shell is obtained around each core particle.

However, traditionally, polymer-based core-shell particles are obtained by interfacial polymerization of the shell-forming monomer onto the core-forming polymer. This process is generally referred to as two-stage or seeded emulsion polymerization. The two-step polymer latex is produced by free radical polymerization of a monomer onto a seed latex. The use of an oil-soluble initiator or a water-soluble initiator will result in grafting due to the formation of radicals on the seed polymer backbone. However, the presence of monomer droplets or micelles may lead to side reactions, e.g. polymerization in secondary nucleated particles. Secondary nucleation not only affects the colloidal stability of the obtained latex product, but the grafting efficiency may also decrease tremendously. Moreover, seeded emulsion polymerizations lead to many different heterogeneous structures. Therefore, a number of parameters including monomer-to-core polymer ratio, polarities of core and shell polymers, and operational details of the polymerization process, have to be taken into account to obtain the desired composite latex particles.

Depending on the applications, the obtained dispersion may then be mixed with another latex, such as a paint for instance, or the particles may be harvested by coagulation or freeze–drying, and then dispersed at specific volume fractions in the material to be toughened.

The work presented in this paper is based on the use of an artificial latex, containing ethylene–propylene copolymers (EPM), ethylene–propylene-diene copolymers (EPDM) or a mixture of both types (EP(D)M), as seed latex in the emulsion polymerization of methyl methacrylate (MMA).

Interfacial adhesion between the rubber phase and the polymer matrix is regarded as playing a significant role in the toughening of the brittle matrix. An improved adhesion leads to enhanced toughness. Therefore, the nature of the matrix considered in the present paper was chosen similar to that of the shell, i.e. PMMA, in order to assure adhesion between the impact modifier and the fragile matrix.

The morphology of the obtained particles will be discussed, using kinetic and thermodynamic considerations for morphology predictions. The mechanism of grafting will be emphasized, taking into account the occurrence of secondary nucleation and its effect on grafting efficiency. Tensile tests as well as scanning electron microscopy (SEM) and transmission electron microscopy (TEM) were used to evaluate the properties of the obtained structured particles incorporated into a PMMA matrix.

2. Experimental section

2.1. Chemicals

Methyl methacrylate (MMA, Aldrich, 99%) was purified by passing it through a column packed with basic aluminum oxide (Aldrich, Brockmann I, standard grade, 150 mesh, 58 Å). Sodium dodecyl benzene sulfonate (SDBS, Fluka, technical grade, 80%), hexadecane (HD, Aldrich, 99%), pentane (Biosolve, AR), divinylbenzene (DVB, Aldrich, technical grade, 80%), poly(1,2-butadiene) (Ricon® 156, Cray Valley), petroleum ether (Biosolve, boiling point ranging from 60 to 80 °C) and acetonitrile (Biosolve, HPLC-S, +99.9%) were used as received.

All other reagents were also used as received, viz. cumene hydroperoxide (CHP, Luperox® CU90, Aldrich, 88%), benzoyl peroxide (BPO, Fluka, 75%), sodium formaldehyde sulfoxylate hydrate (SFS, Fluka, +98%), sodium dodecyl sulfate (SDS, Aldrich, 98%), disodium salt of ethylenediamine tetra-acetic acid (EDTA, Aldrich, +99%), iron (II) sulfate heptahydrate ($FeSO_4$, Aldrich, +99%), sodium persulfate (SPS, Aldrich, reagent grade, +98%), and sodium hydrogen carbonate ($NaHCO_3$, Aldrich, 99%). Deionized water was used in all recipes.

Table 1
Recipe for seed latexes

Seed latex No.	Amount of product (g)						
	Lucant® HC-20	Trilene® 67	HD[a]	DVB	Ricon® 156	Water	SDBS[a]
S1	30.7	3.4	1.2	–	–	104.0	1.1
S2	36.2	3.8	2.0	5.8	16.2	187.4	2.0
S3	33.2	3.5	1.3	3.7	–	104.0	1.2

[a] In water: $[SDBS] \approx 3 \times 10^{-2}$ mol dm^{-3} and $[HD] \approx 4 \times 10^{-2}$ mol dm^{-3}.

The EPM (Lucant® HC-20, Mitsui Chemicals Inc., $\bar{M}_w = 1450$ g mol^{-1}) and the EPDM (Trilene® 67, Crompton Corp., $\bar{M}_w = 28,716$ g mol^{-1}) were described in a previous paper [12].

2.2. Preparation of a seed latex

The preparation of the seed latex has been extensively described earlier [12]. Recipes used in the present work are collected in Table 1. In a first step, SDBS was dissolved in water. A homogeneous mixture of EPM and EPDM was prepared with the help of pentane. After pentane evaporation, hexadecane, DVB and/or poly(1,2-butadiene) (Ricon® 156) were added to the EPM–EPDM mixture. In a second step, the organic phase was brought into the SDBS-containing aqueous phase. The resulting blend was then stirred for one minute with a rotor-stator Ultra-Turrax® T25 Basic at 24.000 rpm. The volume average diameter of the polymer particles was reduced from 20 μm to 360 nm by processing the emulsion product of the Ultra-Turrax® in a Niro-Soavi Lab homogenizer Panda 2 K, operating for 45 min at 1100 bar and with a shear rate of approximately 8.0×10^7 s^{-1}.

Latex S1 was then used without further treatment as seed latex for a seeded emulsion polymerization of MMA. Two homogenizer products were submitted to a crosslinking reaction, as described elsewhere [13], prior to the grafting experiment, giving rise to latexes S2 and S3. Crosslinking was performed using benzoyl peroxide (BPO) as initiator. Both DVB and Ricon® 156 were used as crosslinking promoting co-agents in S2, whereas S3 was obtained in the presence of DVB only.

2.3. Seeded emulsion polymerization of MMA onto EP(D)M

The graft polymerizations were carried out in a 300 ml jacketed-reactor, equipped with a condenser and a down-flow 45° pitched four-blade impeller. Two types of monomer addition were used, i.e. flooded and starved–feed, as indicated in Table 2.

When monomer-flooded conditions were applied, both the EP(D)M seed latex and the monomer were charged into the reaction vessel. After swelling the EP(D)M particles with MMA overnight, the oxygen was removed by purging argon through the mixture for at least 30 min. An aqueous solution of additives, i.e. SFS, EDTA and $FeSO_4$, also referred to as redox system, was charged into the reactor, followed by the addition of the initiator, i.e. cumene hydroperoxide (CHP).

In case of starved–feed conditions, the EP(D)M seed latex was charged into the reaction vessel and purged with argon for at least 30 min to remove the oxygen. MMA and CHP were mixed prior to the addition, to ensure the presence of radicals in the vessel during the complete addition of monomer. The monomer/CHP mixture was continuously added to the reactor at a rate of 0.05 ml min^{-1}, using an automatic burette (Metrohm, type 665 Multi Dosimat, refillable 10 ml-burette).

The polymerization reactions were performed at 50 °C, at a stirring speed of 300 rpm, for at least 5 h. The

Table 2
Recipes for seeded emulsion polymerizations (SEP)

SEP No.	Seed latex				Amount of product (g)				Monomer-to-rubber ratio (g/g)	Reaction time (h)
	No.[a]	Amount (g)	CHP	SFS	EDTA	$FeSO_4$	MMA	Styrene		
SEP1	S1	144.2	0.126	0.084	0.007	0.008	14.9	–	0.8	5.0
SEP2	S1	144.1	0.108	0.115	0.012	0.013	19.2	2.2	0.8	7.3
SEP3[b]	S1	140.5	0.370	0.215	0.022	0.022	33.8	–	1.3	12.4
SEP4[c]	S1	141.2	0.082	0.085	0.007	0.006	23.4	–	0.8	8.0
SEP5	S2	141.5	0.093	0.144	0.018	0.014	19.9	–	0.8	7.0
SEP6	S3	69.2	0.040	0.094	0.007	0.009	12.1	–	0.8	5.0

[a] See Table 1.
[b] In case of SEP3, the monomer-to-EP(D)M ratio was 1.3 instead of 0.8. Therefore, 25 ml of an aqueous solution of SDBS ($[SDBS] \approx 9 \times 10^{-2}$ mol dm^{-3}) was regularly added during the polymerization to maintain the colloidal stability of the latex.
[c] SEP4 was carried out using monomer-flooded conditions instead of starved–feed conditions, as used in all the other cases.

post-treatments included coagulation of the latex using freeze–thaw cycles, and washing the coagulated product with deionized water. The gross polymers were recovered and dried to a constant weight in a vacuum oven at 60 °C.

2.4. Synthesis of a PMMA homopolymer latex

The emulsion homopolymerization of MMA was carried out in a 300 ml jacketed-reactor, equipped with a condenser and a downflow 45° pitched four-blade impeller.

SDS (0.9 g), $NaHCO_3$ (0.2 g), and water (126.2 g) were first charged into the vessel. Oxygen was removed by purging argon through the mixture for at least 30 min. The addition of monomer (59.9 g) was then followed by its emulsification at 60 °C and at a stirring speed of 400 rpm, during 45 min. Finally, the polymerization was initiated by introducing an aqueous solution of SPS (0.2 g in 1 g of water) into the reaction mixture.

2.5. Blending and specimen preparation

Mixing the composite rubber latex and the PMMA homopolymer latex ($\bar{M}_n = 575,000$ g mol^{-1}, $\bar{M}_n = 895,000$ g mol^{-1}) in different weight ratios led to the formation of two new mixed latexes, containing a total EP(D)M weight fraction of 5 and 15 wt%, respectively. After stirring, the homogeneous mixtures were submitted to freeze–drying, leading to white powders. These PMMA/rubber blends were compression molded at 180 °C, under pressures ranging from 40 to 100 bar. The obtained films were then transformed into tensile bars, characterized by a thickness of 0.7 mm.

2.6. Characterization

2.6.1. Particle size distribution

A Coulter LS230 particle sizer was used to verify the colloidal stability of latexes after grafting. This analyzer uses the principles of light scattering, based on both Fraunhofer and Mie theories, to determine particle size distributions.

The lowest size detectable being 40 nm, most of the particles formed by secondary nucleation and observed by cryo-TEM could not be identified.

2.6.2. Grafting efficiency

The gross polymers were separated into graft copolymers, free EP(D)M, and free PMMA by Soxhlet extractions. Petroleum ether, with a boiling point ranging from 60 to 80 °C, and acetonitrile were used for at least 10 h to extract the free rubber and the free PMMA, respectively. The grafting efficiency (GE) may be calculated with:

$$\mathrm{GE} = \frac{\text{weight of MMA grafted}}{\text{weight of MMA polymerized}} \quad (1)$$

2.6.3. Composition of the extracted materials

The materials soluble in acetonitrile were analyzed, after drying, using ^{1}H nuclear magnetic resonance (NMR), on a Varian-300 spectrometer at 25 °C, using TMS as internal standard and $CDCl_3$ as solvent.

2.6.4. Thermal properties

Thermal characterization of dried latexes was performed by temperature modulated-differential scanning calorimetry (TM-DSC). Analyses were carried out on a modified Perkin–Elmer DSC-7 differential scanning calorimeter, equipped with a function generator for sinusoidal temperature modulation.

The measurements were carried out in a nitrogen atmosphere to prevent degradation of the polymer samples. Standard aluminum pans of similar predetermined mass were used for all measurements. The pans masses on the reference side and sample side were balanced to give a zero signal for the baseline. Every sample typically consisted of approximately 2 mg of polymer.

The experiments were carried out in a heating cooling mode, using a temperature amplitude of 0.3 K and a frequency of 25 and 12.5 mHz, i.e. 40 and 80 s period, respectively. The equipment was operated at temperatures ranging from −100 to 130 or 150 °C, and with an underlying heating rate β_0 of 2 K min^{-1}.

The measured heat flow rate consists of two parts [14]: a non-periodic underlying part $\Phi_u(t)$ and a periodic part $\Phi_{per}(T,t)$. A so-called 'gliding integration' of the signal over one period provides the underlying part $\Phi_u(t)$. Subtracting $\Phi_u(t)$ from the total measured signal yields the periodic part $\Phi_{per}(T,t)$. The specific heat capacity c_p (magnitude and phase shift) is then calculated using a mathematical procedure described in the literature [14,15]. Glass transition temperatures and Δc_p were determined using conventional methods [16].

2.6.5. Minimum film formation temperature (MFFT)

Thick films (200 μm) were drawn from various latexes on an MFFT bar from Sheen Instruments. The minimum film formation temperature corresponds to the temperature at which a white, powdery, cracked film becomes clear and transparent.

2.6.6. Molecular weight and molecular weight distribution

Molecular weight (MW) and molecular weight distribution (MWD) were determined at ambient temperature, using a waters size exclusion chromatograph (SEC), equipped with a Waters model 510 pump, a Waters 410 differential refractometer operating at 40 °C and a Waters model 486 UV detector operating at 254 nm. Samples were injected using a Waters WISP 712 autoinjector (50 μl injection volume). The columns consisted of a PL gel guard (5 μm particles) 50×7.5 mm (L×ID) column, followed by two PL gel mixed-C or mixed-D (5 μm particles) 300×7.5 mm (L×ID) columns at 40 °C in series. The eluent was THF, and the elution volumetric flow rate was maintained at 1 ml min^{-1}. Calibration was carried out using narrow

MWD polystyrene standards ranging from 580 to 7×10^6 g mol^{-1}.

2.6.7. Particles morphology

The morphology of the particles was examined using cryo-transmission electron microscopy (cryo-TEM). For the present work, the use of cryo-TEM was required because of the low glass transition temperature of the EP(D)M phase.

To perform cryo-TEM analysis, each latex sample was applied onto a microscopy grid. The thin aqueous film obtained was then vitrified in liquid ethane before being transferred to a Philips CM12 microscope, for examination at liquid nitrogen temperature. Dehydration and major reorganization of the latex particles were prevented by the low temperature.

2.6.8. Surface and interfacial tension measurements

Surface properties of both EP(D)M and PMMA as well as of the water phase are required for the prediction of particle morphology, as described in the next sections. Note that pure deionized water and surfactant-containing water exhibit different surface properties. Therefore, all measurements including water were carried out using an aqueous solution of SDBS, in which the SDBS concentration was similar to the one usually used in latexes, i.e. 3×10^{-2} mol dm^{-3}.

The interfacial tension between EP(D)M and SDBS-containing water ($\gamma_{\text{EP(D)M-water/SDBS}}$) was determined with a Krüss G10 goniometer, using the pendant drop method.

Other interfacial tensions, i.e. between PMMA and SDBS-containing water ($\gamma_{\text{PMMA–water/SDBS}}$), as well as between EP(D)M and PMMA ($\gamma_{\text{EP(D)M–PMMA}}$), were calculated using the modified Young's equation [17], also called geometric-mean equation [17,18]:

$$\gamma_{12} = \gamma_1 + \gamma_2 - 2\left(\gamma_1^d\gamma_2^d\right)^{1/2} - 2\left(\gamma_1^p\gamma_2^p\right)^{1/2} \tag{2}$$

where γ_1 is the surface tension of phase 1, γ_2 is the surface tension of phase 2, and γ_{12} is the interfacial tension between phases 1 and 2. In the above equation, γ_1^d and γ_2^d are the dispersive components of the surface tensions of materials 1 and 2, while γ_1^p and γ_2^p are the respective polar components. As suggested by Fowkes [19], these two components are related as

$$\gamma_i = \gamma_i^d + \gamma_i^p \tag{3}$$

Contact angles of water and methylene iodide were measured on EP(D)M and PMMA spin-coated films, using the Krüss G10 goniometer. Surface free energies of EP(D)M and PMMA were then evaluated using the Owens–Wendt method [20].

Surface tension of SDBS-containing water was determined on a Krüss K100 tensiometer, equipped with a platinum plate, using the Wilhelmy plate method. Both polar and dispersive components were evaluated, using poly(tetrafluoroethylene) (PTFE) as standard reference surface, as reported in a Krüss technical note [21].

2.6.9. Tensile properties

Tensile tests were performed on a Zwick Z010 tensile-testing machine, based on ISO standard 527, at room temperature. The strain speed was 1 mm min^{-1}. The elongation was measured directly on the sample by a tensometer. The tensile curves represent the average data points of five measurements.

2.6.10. Micro-morphology

The dispersion of the rubbery particles in the PMMA matrix was observed on non-elongated samples by transmission electron microscopy (TEM). Samples were trimmed at low temperature to achieve a smooth undeformed surface and subsequently treated during 20 h with a ruthenium tetraoxide (RuO_4)-solution [22]. Ultra-thin sections were obtained at room temperature using a Reichert Ultracut E microtome, equipped with a diamond knife. TEM was performed using a Jeol JEM 2000 FX microscope, operated at 80 kV.

After tensile tests, the fracture surfaces of the specimens were examined with a Philips XL30 field emission gun-environmental scanning electron microscope (FEG-ESEM). Samples were coated with a thin gold layer, using an Emitech K575X sputter-coater.

3. Results and discussion

3.1. Grafting mechanism

Grafting of MMA onto EP(D)M-based latex particles was carried out using cumene hydroperoxide (CHP) combined with sodium formaldehyde sulfoxylate hydrate (SFS, H_2O)/EDTA-chelated Fe^{2+} as redox initiation system [23]. A mechanism of grafting has been reported by Arayapranee et al. [24] for the graft polymerization of the monomer pair styrene/MMA onto natural rubber. Adapting their approach to our system, a mechanism for the graft polymerization of MMA onto EP(D)M is suggested in the present section.

Most of the free radicals are produced at the monomer-swollen particle/water interface, since the peroxide is soluble in the organic phase, whereas the iron/EDTA complex is water-soluble. Therefore, the surface of the particle becomes the locus of polymerization. Peroxy radicals may react with the EP(D)M backbone, leading to a macroradical that will initiate grafting. However, the same peroxy radical may also initiate MMA, resulting in homopolymerization in the aqueous phase followed by secondary homogeneous particle nucleation. PMMA macroradicals may either recombine with EP(D)M radicals to terminate, leading to graft copolymers, or transfer to EP(D)M or monomer leading to free PMMA. Finally, two

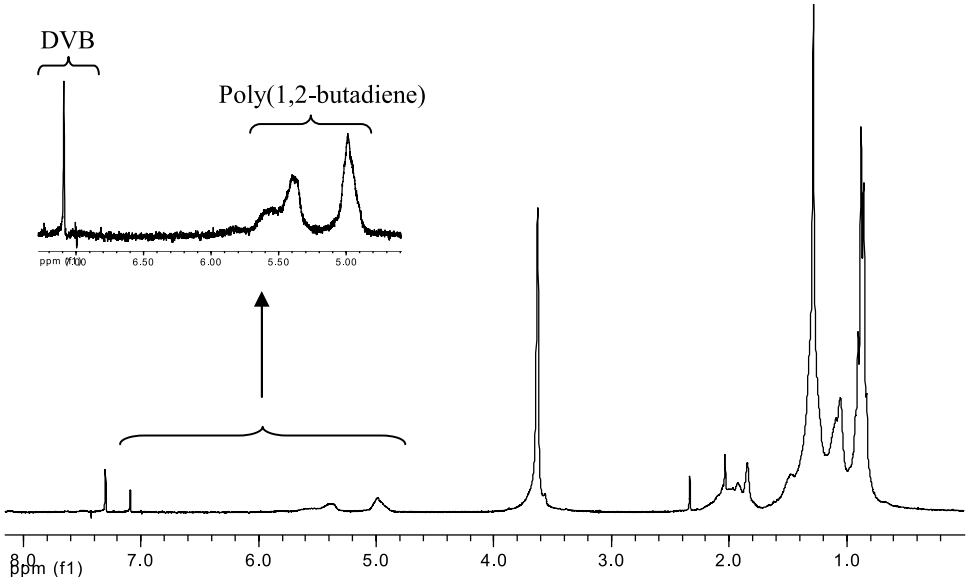

Fig. 2. ^{1}H NMR spectrum of PMMA extracted with acetonitrile. DVB and poly(1,2-butadiene) are also present in the extracted phase. Therefore, Soxhlet extraction is not the right method to quantify the grafting efficiency.

rubber radicals may also recombine leading to partial crosslinking of the starting seed latex particles.

So, in the present work, a step forward would be made if the homopolymerization of MMA via secondary nucleation could be minimized, if not avoided. As a consequence, several conditions were applied to the present seeded emulsion polymerizations, i.e.:

- The monomer was starved–feed in most experiments to minimize propagation in the aqueous phase [25].
- The use of both cumene hydroperoxide and a redox initiation system, i.e. SFS, EDTA and $FeSO_4$, is expected to favor reactions inside the EP(D)M particles or near their surface.
- The surfactant concentration was kept below its critical micelle concentration (CMC) in the latex to minimize homogeneous nucleation.

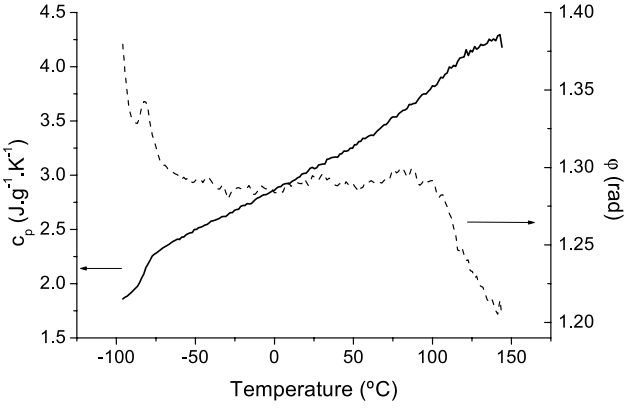

Fig. 3. Specific heat capacity (c_p) and phase angle (ϕ) of SEP5, after drying, obtained by TM-DSC.

3.2. Efficiency of the grafting reaction

3.2.1. Grafting efficiency

The grafting efficiency of the various seeded emulsion polymerizations of MMA onto EP(D)M particles could not be determined using classical Soxhlet extractions. Indeed, although acetonitrile leads to the extraction of pure PMMA obtained by secondary nucleation, this solvent also leads to the extraction of PMMA-*g*-EP(D)M copolymers containing divinylbenzene (DVB) and poly(1,2-butadiene) (Ricon® 156), as indicated by the ^{1}H NMR spectrum of an extracted product, see Fig. 2.

3.2.2. Thermal properties

Since Soxhlet extractions were not successful, Temperature modulated-differential scanning calorimetry (TM-DSC) was used to acquire more information about the grafted material, obtained by seeded emulsion polymerization of MMA onto the EP(D)M particles.

Fig. 3 shows an example of TM-DSC result, with at least two glass transitions, i.e. a sharp one at −80 °C and a broad one at +90 °C. A third very weak glass transition seems to appear at +26 °C. As observed in this thermogram of SEP5, the step-like change of the real part of the complex heat capacity $c_p(\omega)$, in the glass transition region, is always coupled with a maximum of the imaginary part, i.e. the phase ϕ_{max}. The maximum in the phase signal is usually more visible than the step change in the c_p curve (or in conventional thermograms). This is one advantage of the TM-DSC method against conventional DSC.

Following these observations, the glass transition at −80 °C clearly indicates the presence of rubber domains. The broader glass transition in the range of 50–120 °C may be due to the overlapping of two consecutive glass

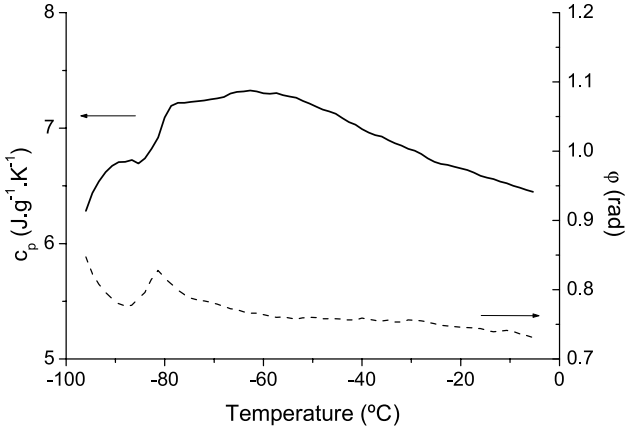

Fig. 4. Specific heat capacity (c_p) and phase angle (ϕ) of a pure EP(D)M sample, obtained by TM-DSC.

transitions. Indeed, one T_g at 106 °C characterizes PMMA. The presence of another T_g of lower value may be explained by PMMA segments grafted onto EP(D)M chains. This may also explain the third glass transition observed in the region of 25 °C.

However, the broadness of a glass transition region may also find explanation in the existence of polymer chains exhibiting different molar masses. It is indeed recognized that small molecules may act as solvent or plasticizer, causing a decrease of the glass transition temperature. A distribution of molar mass or a distribution of various domains may lead to a continuous distribution of T_g's and, therefore, to a broad glass transition region, as observed in Fig. 3. For the present research, samples were investigated using size exclusion chromatography. A large polydispersity index of 2.6 confirmed the presence of small and long chains in the studied system.

Moreover, the contribution of EP(D)M in the grafting process may be determined by a quantitative analysis of the thermogram. The TM-DSC analysis of pure EP(D)M showed a variation of c_p, namely a $\Delta c_{p,th}$, of 0.53 J g^{-1} K^{-1}, as depicted in Fig. 4. The T_g of −80 °C, observed in Fig. 3 is characteristic of the fraction of EP(D)M that is not involved in the grafting process. The Δc_p value corresponding to this transition, i.e. the average Δc_p calculated from five different TM-DSC curves, is 0.22 J g^{-1} K^{-1}. This Δc_p step is less significant than the one observed for pure EP(D)M, since the fraction of EP(D)M involved in grafting does not contribute to this glass transition anymore. Eq. 4 can then be used to determine the weight fraction of EP(D)M

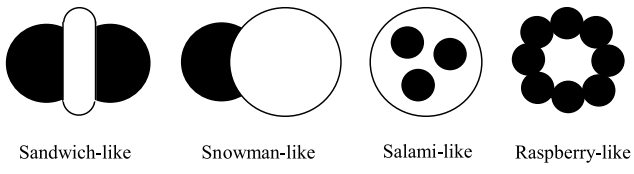

Fig. 5. Possible phase-separated morphologies, where (□) represents the first-stage polymer, and (■) the second-stage polymer.

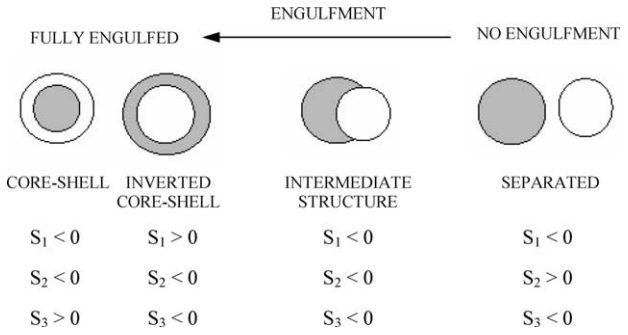

Fig. 6. Engulfment and spreading coefficients.

phase involved in the grafting process, i.e. approximately 22%:

$$\%\ \text{Grafted EP(D)M} = \left(1 - \frac{\Delta c_p}{f_{EP(D)M}\Delta c_{p,th}}\right) \times 100 \qquad (4)$$

where $f_{EP(D)M} = 0.53$ represents the weight fraction of EP(D)M in the sample, determined with the recipe, $\Delta c_p = 0.22$ the measured step height, and $\Delta c_{p,th} = 0.53$ the step height of pure EP(D)M.

3.3. Morphology of the EP(D)M-g-PMMA particles

3.3.1. Morphology predictions

Two-stage emulsion polymerization produces heterogeneous structures such as core-shell [26,27], 'inverted' core-shell [28,29] and phase-separated structures. Phase-separated morphologies include 'sandwich-like' [30], 'snowman-like' [31], 'salami-like' [32], and 'raspberry-like' [33] particles, as exemplified in Fig. 5.

The particle morphology may be affected by many polymerization parameters, e.g. initiator, surfactant, monomer-to-seed polymer ratio, as mentioned earlier. Therefore, predicting particle morphology using thermodynamic and kinetic considerations may help understanding the structure of the final composite latex particles.

3.3.1.1. Thermodynamic considerations. A method for the thermodynamic approach of morphology prediction was first reported in 1970 by Torza and Mason [34], who considered two immiscible liquids dispersed in a third immiscible liquid, i.e. water. Since then, numerous researchers tried to extend this concept to various encapsulating systems. Chen et al. [35] described the morphology changes occurring during the batch seeded emulsion polymerization of MMA onto polystyrene, in terms of free energy changes. The thermodynamically preferred morphology is the one that has the lowest interfacial free energy. Waters [36,37] investigated the evolution of interfacial energy from separated structures to fully engulfed particles and was able to determine the degree of engulfment corresponding to minimum interfacial energy.

Table 3
Measured surface tensions of the various components of a latex

Material	Surface tensions (mN m^{-1})		
	γ	γ^d	γ^p
Water + SDBS	30.4	26.0	4.45
PMMA	42.7	38.0	4.7
EP(D)M	29.3	27.3	2.0

In the present work, the morphology of the particles produced during the seeded emulsion polymerization of MMA onto EP(D)M was predicted using both theories of Torza/Mason [34] and Waters [36,37].

Torza and Mason [34] defined the spreading coefficients, S_i, of a three-phase system as:

$$S_i = \gamma_{jk} - (\gamma_{ij} + \gamma_{ik}) \tag{5}$$

where γ is the interfacial tension and i, j, and k are the three phases considered. The different possible structures and their various spreading coefficients are depicted in Fig. 6.

By convention [34], phase 1 must be the phase for which $\gamma_{12} > \gamma_{23}$, so that $S_1 < 0$. Then, complete engulfment, i.e. core-shell, occurs when $S_2 < 0$ and $S_3 > 0$. However, if $S_2 < 0$ and $S_3 < 0$, the engulfment is only partial and leads to hemispherical, also called acorn or snowman morphologies. Finally, when $S_2 > 0$ and $S_3 < 0$, separated structures are preferred.

For the investigated system, the continuous phase (water, w), EP(D)M and PMMA were designated as phase 2, 1 and 3, respectively. The reason for this assignment is that it fulfills the requirement $\gamma_{12} > \gamma_{23}$. Surface tensions of SDBS-containing water and both polymers, collected in Table 3, were used for the determination of the various interfacial tensions. As demonstrated in Table 4, the calculated spreading coefficients predict a core-shell morphology for the particles produced during the seeded emulsion polymerization of MMA onto EP(D)M latex, since $S_1 < 0$, $S_2 < 0$, and $S_3 > 0$.

The morphology predictions obtained with the Torza/-Mason theory were verified using the quantification of relative surface energies, as suggested by Waters [36,37]. Considering an engulfed polymer Q by a polymer P, fully engulfed structures are favored over any intermediate or separated structures if:

$$\frac{\gamma_{Q-W} - \gamma_{P-Q}}{\gamma_{P-W}} > 1 \tag{6}$$

where γ is the interfacial energy for the interfaces polymer Q–water, polymer P–water, and polymer Q–polymer P.

It is then possible to determine which morphology, either core-shell or inverted core-shell, is thermodynamically favored, by considering the fractional volumes, ν_P and ν_Q, of both polymers. Waters showed that a core-shell particle should be expected when the following condition is obeyed:

$$\frac{\gamma_{Q-W} - \gamma_{P-W}}{\gamma_{P-Q}} > \nu_Q^{2/3} - \nu_P^{2/3} \tag{7}$$

In the present work, polymers Q and P correspond to EP(D)M and PMMA, respectively.

The data in Table 5 confirm that, for our system, the core-shell morphology is to be expected, as was also predicted by the Torza/Mason theory.

3.3.1.2. Kinetic considerations. According to Sundberg [38], several morphologies (hemispherical, sandwich, multiple lobes) can coexist within a single (sub)micron dispersion, suggesting that they may simply represent different states of phase separation and are only metastable morphologies. In that case, the morphology is, therefore, governed by kinetics, i.e. by the diffusion of polymer chains through the more or less viscous core-forming material. So the viscosity of the polymerization loci represents another key parameter in the determination of the final morphology of latex particles.

As mentioned by van Zyl [39] and González-Ortiz et al. [40–42], during a seeded emulsion polymerization, polymer chains are formed at various positions in the seed particles. However, in the case of a low local viscosity, incompatibility of the newly formed polymer and the seed polymer often leads to phase separation. On the other hand, a high local viscosity prevents the polymer chains from diffusing through the seed particles, minimizing the occurrence of phase separation.

The large influence of local viscosity on the particle morphology was further emphasized by Mills et al. in 1990 [43]. Mills et al. reported significant inhomogeneities in latex particles at high monomer conversion, particularly for large particles. These heterogeneities may be explained by a slow diffusion of free radicals through the core material, due to a high viscosity of the polymerization loci, thereby leading to the formation of core-shell structures.

Finally, as reported by Chern et al. [44–46], free radicals produced during an emulsion polymerization are partially hydrophilic. As a consequence, free radicals are preferably located near the particle surface, leading to a non-uniform distribution of free radicals in the latex particles. A core-shell structure may then be the result of such non-uniform distribution of radicals. In the present work, the

Table 4
Interfacial tensions and spreading coefficients used in the Torza/Mason theory [34]

Interfacial tensions (mN m^{-1})			Spreading coefficients		
$\gamma_{EP(D)M-water}$ (γ_{12} or γ_{Q-W})	$\gamma_{PMMA-water}$ (γ_{23} or γ_{P-W})	$\gamma_{EP(D)M-PMMA}$ (γ_{13} or γ_{Q-P})	S_1	S_2	S_3
3.7	1.2	1.5	−4.0	−3.4	1.1

Table 5
Interfacial tensions and conditions for morphology predictions according to Waters [36,37]

Interfacial tensions (mN m^{-1})			Conditions		
$\gamma_{EP(D)M-water}$ (γ_{Q-W})	$\gamma_{PMMA-water}$ (γ_{P-W})	$\gamma_{EP(D)M-PMMA}$ (γ_{Q-P})	$(\gamma_{Q-W}-\gamma_{P-Q})/\gamma_{P-W}$	$(\gamma_{Q-W}-\gamma_{P-W})/\gamma_{P-Q}$	$\nu_Q^{2/3}-\nu_P^{2/3}$
3.7	1.2	1.5	1.8	1.7	0.3

hydrophilicity of the redox part should prevent the peroxide from being buried inside EP(D)M seed particles, therefore, also favoring core-shell structures.

3.3.2. Influence of various parameters on particle morphology

Several parameters were studied in the present research to understand the chemistry involved in the procedure of producing core-shell impact modifiers, based on an EP(D)M core and a PMMA shell.

Note that the particle size distributions of the latexes before and after grafting were similar and also point to a sufficient colloidal stability, as observed in Fig. 7. However, a monomer-to-rubber ratio larger than 0.8 required the addition of an aqueous solution of SDBS, to ensure the colloidal stability of the latex particles, as mentioned in Table 2.

In order to clearly differentiate EP(D)M from PMMA in cryo-TEM pictures presented further on, a pure EP(D)M latex and a physical mixture of both an EP(D)M latex and a PMMA latex are depicted in Figs. 8 and 9, respectively. EP(D)M particles exhibit a sharp edge and seem to exhibit a perfect spherical shape, while PMMA particles appear more fluffy. Moreover, the higher electron density of PMMA compared to EP(D)M emphasizes the darkness of the PMMA phase, as depicted in Fig. 9.

3.3.2.1. Monomer type. Seeded emulsion polymerization SEP1 was carried out under starved–feed conditions and using a monomer-to-rubber ratio of 0.8 (wt/wt), as presented in Table 2. SEP1 leads to the formation of two types of particles, as depicted in Fig. 10. A minority of small particles of pure PMMA was formed by secondary nucleation, whereas grafting of monomer onto the EP(D)M seed latex gave rise to snowman-like particles. Styrene was then introduced in small quantities (SEP2) in order to form more hydrophobic copolymers of MMA and styrene [47]. Unfortunately, using a combination of MMA and styrene in SEP2 does not produce core-shell structures either, as depicted in Fig. 11. From this, we conclude that the different hydrophilicity of both the homopolymer PMMA and the styrene/MMA copolymer as well as that of the rubber is not the driving force to obtain core-shell morphology.

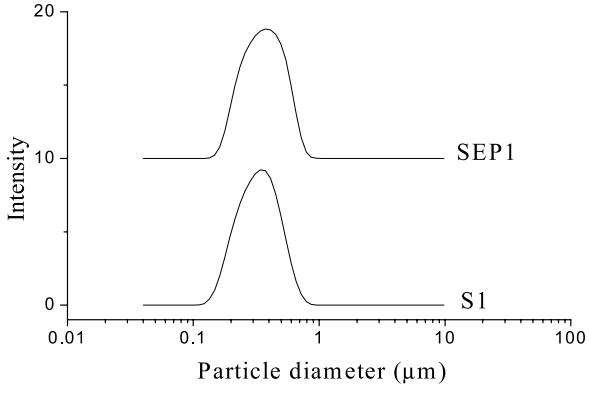

Fig. 7. Particle size distribution obtained for a latex before (S1) and after (SEP1) grafting.

3.3.2.2. Monomer-to-rubber ratio. The quantity of monomer, i.e. MMA only or a mixture of styrene and MMA, may be too small to completely cover the EP(D)M particles, which may explain the formation of unexpected snowman-like structures. The monomer-to-rubber ratio was, therefore, raised from 0.8 to 1.3, as indicated in Table 2. Note the presence of a larger amount of small particles, i.e. characterized by a diameter of 20–50 nm, produced by secondary nucleation, see Fig. 12. Snowman-like morphologies, exhibiting a much larger PMMA phase (dark and fluffy) than in Fig. 10, can clearly be observed. Complete coverage of the EP(D)M particles by PMMA was still not achieved.

3.3.2.3. Monomer feed type. In addition to the monomer type and to the monomer-to-rubber ratio, the influence of the monomer feed type, i.e. flooded or starved–feed, was investigated. As observed in Fig. 10, starved–feed

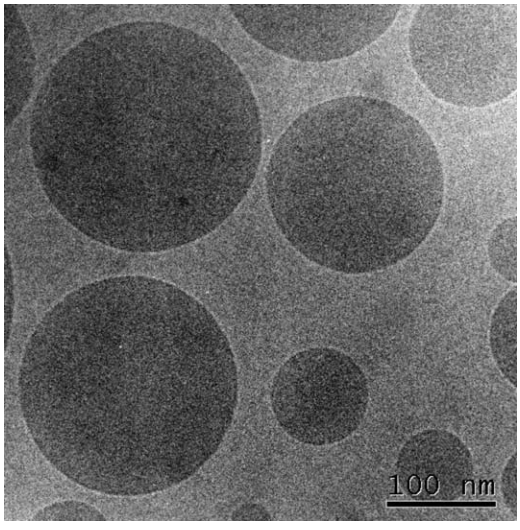

Fig. 8. Cryo-TEM picture of a pure EP(D)M seed latex (S1).

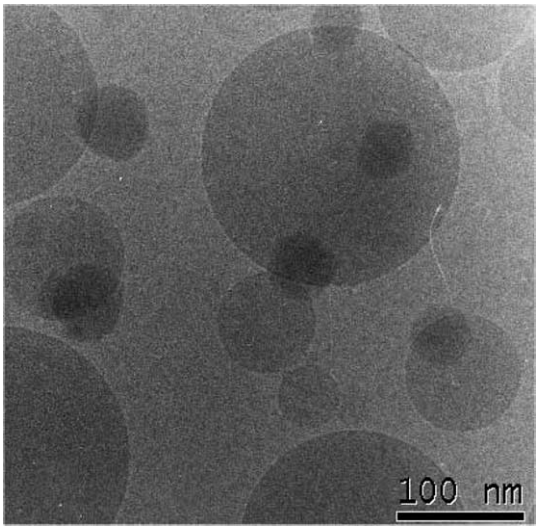

Fig. 9. Cryo-TEM picture of a physical mixture of both an EP(D)M latex (*S*1) and a PMMA latex.

conditions lead to the formation of snowman-like particles. Monomer-flooded conditions, on the other hand, gave rise to inverted core-shell particles, as depicted in Fig. 13 for SEP4. These inverted core-shell structures consist of a dark PMMA core and a relatively sharp-edged EP(D)M shell, see Fig. 13(a). Many secondary nucleated PMMA particles were also produced, as depicted in Fig. 13(b).

During this experiment, most of the MMA entered the EP(D)M particles while a smaller fraction, typically 1.56 wt% [48], was present in the aqueous phase. Moreover, although the initiator, i.e. CHP, is mostly water-insoluble, partitioning occurs, leading to a gradient of radicals inside the EP(D)M particles. As a consequence, both monomer and initiator radicals coexist in the rubbery particles, leading to the polymerization of MMA within these rubbery particles, and, therefore, to the formation of inverted core-shell

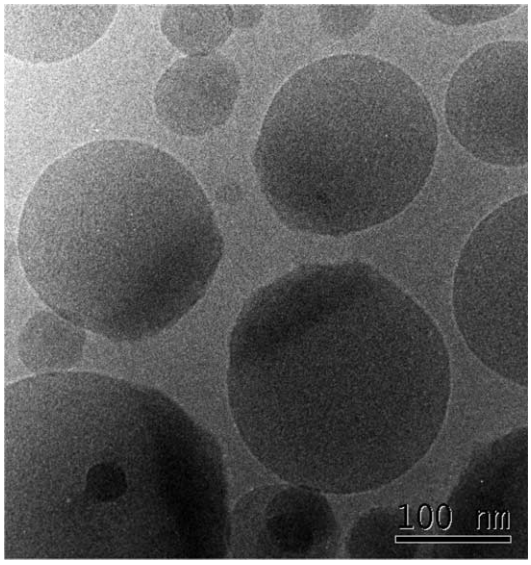

Fig. 10. Cryo-TEM picture of SEP1 (PMMA-to-EP(D)M ratio = 0.8).

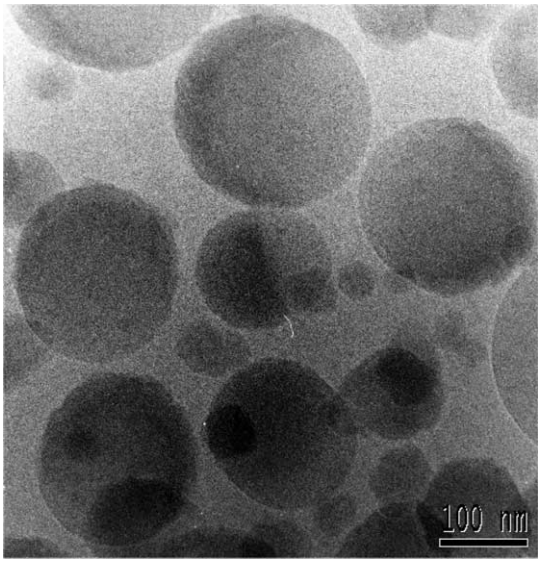

Fig. 11. Cryo-TEM picture of SEP2, consisting of P(MMA-*co*-styrene) (90/10 wt/wt) grafted onto EP(D)M particles.

structures. In this specific case, the morphology of the obtained composite particles is, therefore, determined by the kinetics of the reaction.

3.3.2.4. Crosslinking of the EP(D)M seed particles. Finally, the last parameter investigated consisted of the crosslinking of the EP(D)M seed particles, in the presence or absence of poly(1,2-butadiene) (Ricon® 156). Two seeded emulsion polymerizations (SEP) of MMA were carried out. SEP5 was performed on an EP(D)M seed latex, crosslinked with benzoyl peroxide (BPO) as initiator, in the presence of both divinylbenzene (DVB) and Ricon® 156 as crosslinking co-agents. SEP6 was completed in the same conditions, using

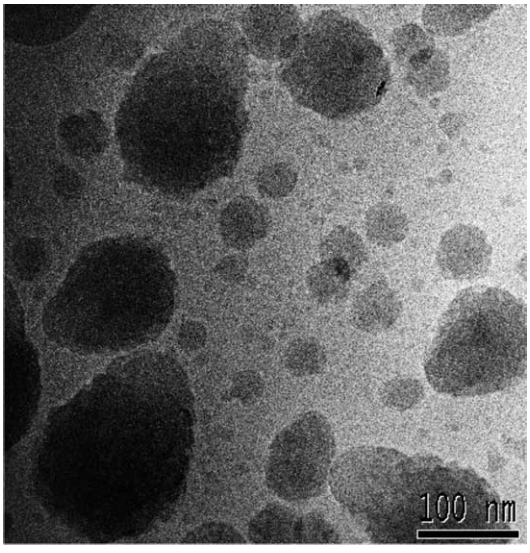

Fig. 12. Cryo-TEM picture of SEP3, consisting of PMMA-*g*-EP(D)M particles. The PMMA-to-EP(D)M ratio is 1.3. Small particles of pure PMMA were formed by secondary nucleation.

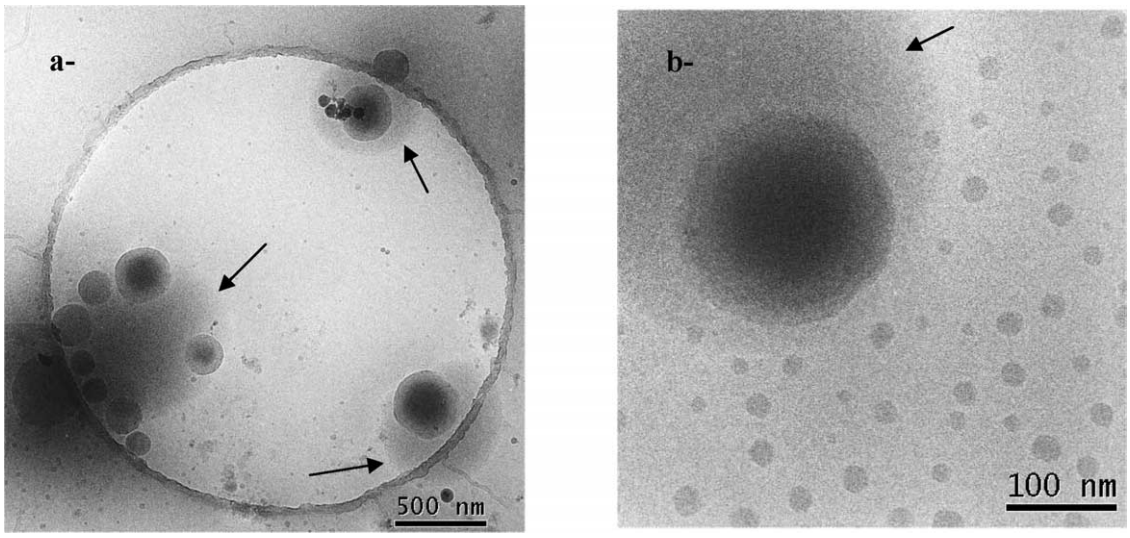

Fig. 13. Cryo-TEM pictures of SEP4, containing EP(D)M-*g*-PMMA particles, obtained in monomer-flooded conditions. The arrows pointing to dark clouds indicate non-polymerized monomer. In Fig. 13(b), small particles of pure PMMA formed by secondary nucleation can be distinguished.

DVB as the only co-agent. The latexes used as seed for SEP5 and SEP6 exhibited a gel content of approximately 21 and 13%, respectively. The structures obtained for SEP5 and SEP6 are presented in Figs. 14 and 15, respectively. The fluffy outer shell is a typical representation of PMMA in cryo-TEM pictures, as previously stated. Therefore, Figs. 14 and 15 clearly demonstrate that a crosslinked EP(D)M seed latex is required for the formation of core-shell structures. Note that pendant polybutadiene unsaturations are not necessary to promote grafting of PMMA onto EP(D)M particles, as depicted in Fig. 15.

Furthermore, a thorough analysis of various cryo-TEM pictures leads to the conclusion that particles from SEP5 consist of approximately 76 vol% of EP(D)M and 24 vol% of PMMA shell.

The formation of snowman-like structures, as in Figs. 10 and 12, as well as the formation of core-shell structures, as in Figs. 14 and 15, may be explained by the relative difference of viscosity between EP(D)M and PMMA. Indeed, when a non-crosslinked EP(D)M latex is used, the soft and flowing EP(D)M chains tend to deform and are then expelled from the (hard) growing PMMA shell. EP(D)M crosslinking hampers the mobility of the EP(D)M chains, therefore, preventing the particles from deformation. However, during a seeded emulsion polymerization carried out with monomer-flooded conditions, the PMMA chains grow within the soft EP(D)M particles, hence forming a core inside the EP(D)M shell.

Note that the formation of core-shell structures was confirmed by minimum film formation temperature (MFFT) measurements. Thus, a latex based on snowman-like or

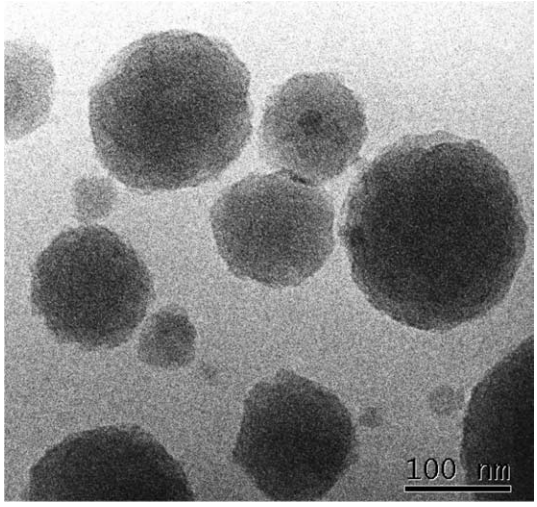

Fig. 14. Cryo-TEM picture of SEP5. The EP(D)M latex was crosslinked with BPO in the presence of DVB and poly(1,2-butadiene) prior to the grafting reaction (gel content ≈ 21%).

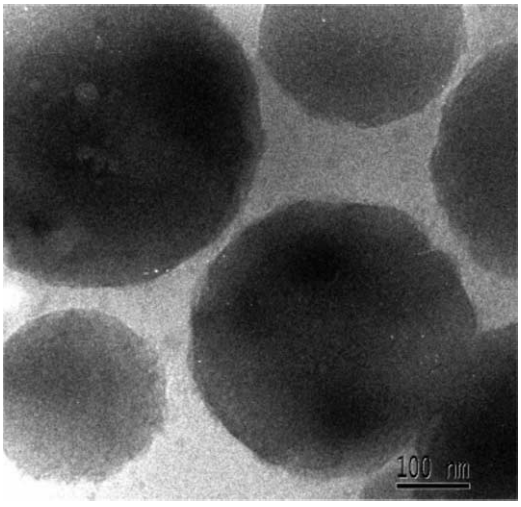

Fig. 15. Cryo-TEM picture of SEP6. The EP(D)M latex was crosslinked with BPO in the presence of DVB only prior to the grafting reaction (gel content ≈ 13%).

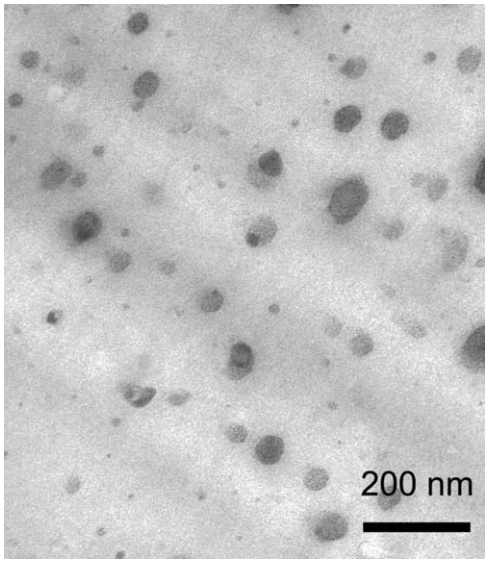

Fig. 16. TEM section of a sample containing 5 wt% of EP(D)M dispersed in a PMMA matrix.

inverted core-shell particles has a much lower MFFT, i.e. 7 °C, than a latex containing core-shell particles with EP(D)M as core, i.e. 74 °C.

3.4. Mechanical properties of PMMA/rubber blends

3.4.1. Incorporation of the rubbery particles into a PMMA matrix

TEM pictures of the samples containing 5 and 15 wt% of rubber are depicted in Figs. 16 and 17, respectively. These pictures demonstrate that the rubbery particles seem more homogeneously dispersed in the sample containing 5 wt% of rubber. Not only single particles but also agglomerates can be distinguished in the sample containing 15 wt% of rubber, see Fig. 17. However, as reported in the next sections, these agglomerates do not seem to affect the tensile properties of the studied samples to a large extent.

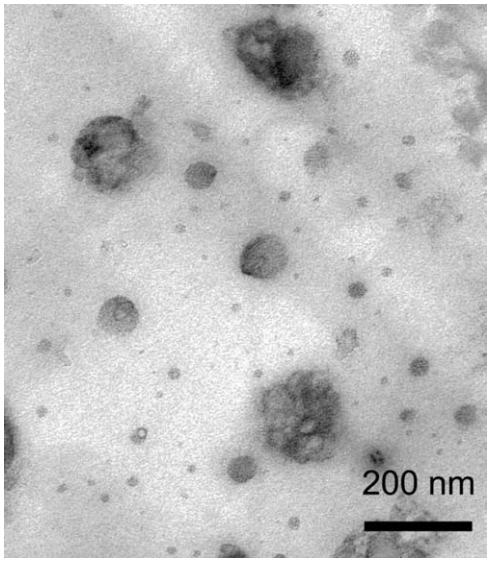

Fig. 17. TEM section of a sample containing 15 wt% of EP(D)M dispersed in a PMMA matrix.

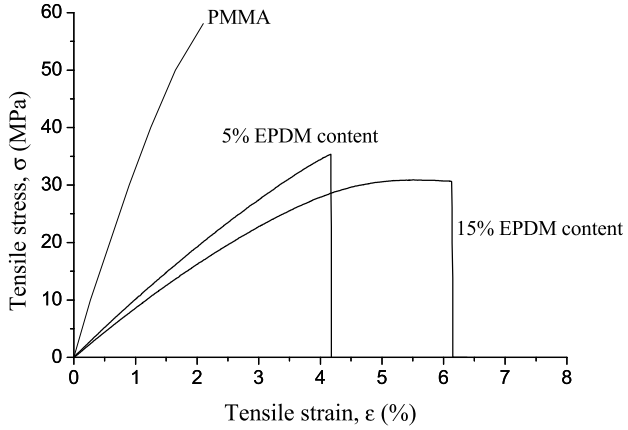

Fig. 18. Stress–strain curves of PMMA toughened by different amounts of EP(D)M–PMMA core-shell particles. Note that the pure PMMA curve was obtained from literature [49].

3.4.2. Tensile properties

Characterization of pure PMMA samples with tensile tests could not be performed, since samples either slipped between the clamps of the machine or were damaged by them. Therefore, it is only possible to compare the data of the present PMMA/rubber blends with those of pure PMMA obtained from literature [49]. Obviously, the blends containing various amounts of rubber can also be compared with each other. Note that the stress–strain curve of PMMA obtained from literature, see Fig. 18, most likely corresponds to the upper stiffness limit for our pure PMMA sample, whereas the curve obtained for the sample containing 5 wt% of rubber, corresponds approximately to the lower limit.

As demonstrated by the stress–strain curves in Fig. 18, the ductility of a brittle PMMA matrix is significantly enhanced by the incorporation of an increasing amount of rubber into the PMMA matrix, in the form of core-shell particles. It should be mentioned here that the incorporation of snowman-like EP(D)M-*g*-PMMA particles, as opposed to core-shell particles, gives rise to sticky tensile specimens. Therefore, encapsulation of the EP(D)M phase by a PMMA shell is required to obtain satisfactory surface properties of the samples.

As reported by Schneider et al. [50], the Young's modulus, E, is controlled by the rubber content of the blends. This statement is confirmed by Fig. 18, where the slope of the stress–strain curves, i.e. the Young's modulus, significantly decreases with increasing amounts of EP(D)M in the PMMA matrix.

Simultaneously, the tensile strain increases from approximately 2% for pure PMMA to 4% for a 5% EP(D)M-based sample, and to 6% for an EP(D)M content of 15%.

Moreover, the surface area under the stress–strain curve,

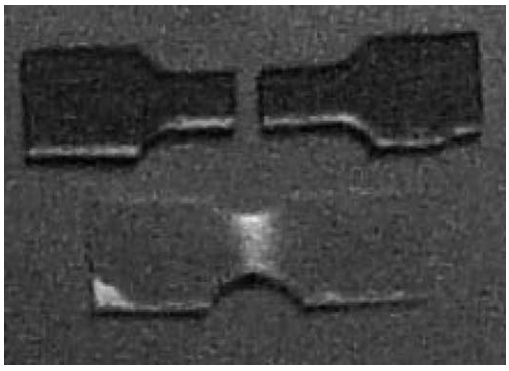

Fig. 19. Tensile bars after bending. The pure PMMA (top) specimen was broken in a brittle way, without any stress-whitening. The toughened material (bottom) shows stress-whitening in its center.

which is a measure for the toughness of the material, is clearly enlarged by the increasing rubber content, see Fig. 18.

Finally, tensile stress and bending of the test bars lead to the formation of white shear bands, as observed in Fig. 19. Stress-whitening, which results from plastic deformation, is usually regarded as a characteristic for deformation of tough materials [51,52]. Hence, the ductility of the material clearly increases with an increasing rubber content. The designed core-shell structures thus provide the desired toughness enhancement.

3.4.3. Fracture mechanism

Scanning electron microscopy (SEM) was performed to relate the results of the tensile tests to the morphology of the multiphase materials produced. Figs. 20 and 21 present the fracture surface of two PMMA/rubber blends containing 5 and 15 wt% of EP(D)M, respectively.

The roughness of the fracture surfaces, including holes and dome-like features, can clearly be observed in the SEM micrographs. These holes correspond to the space occupied by the rubbery particles in the PMMA matrix. Severe plastic deformation occurred around the particles during tensile tests, removing the rubber particles from their original position. This fracture mechanism is usually referred to as debonding or cavitation [53]. The rubber particles, acting as stress concentrators, relieve the tension by cavitation processes. As a consequence, these particles produce extensive matrix deformation by crazing or shear yielding.

The presence of a larger amount of rubber particles in the blend results in a reduced distance between particles [49]. Therefore, an overlap of the stress fields occurs, leading to particle cavitation at lower externally applied stress. The PMMA blend may then be deformed more extensively, as observed in the stress–strain curves in Fig. 18.

Note that, the magnifications being identical for both micrographs, the voids appear larger in Fig. 21 than in Fig. 20. This may be explained by the agglomerates observed in Fig. 17 or by the proximity of rubbery particles, which may form larger holes by coalescence in the brittle PMMA matrix during the deformation process.

In the past, the results of various investigations [54,55] demonstrated that shear yielding was the dominant mechanism of tensile deformation of PMMA, resulting in shear bands as observed in the present study. Later on, Franck and Lehmann [56] emphasized the influence of the strain rates. Hence, at low strain rates, i.e. 0.5% min^{-1}, shear yielding is the main mechanism of deformation, cavitation contributing only to a small extent. However, at higher strain rates, i.e. 10% min^{-1} and higher, the contribution of cavitation processes increases, which consequently leads to a deformation by crazing.

In the present paper, the SEM micrographs indicate that stress-whitening arises from debonding and cavitation of the toughening particles, as was observed by Lovell et al. [52].

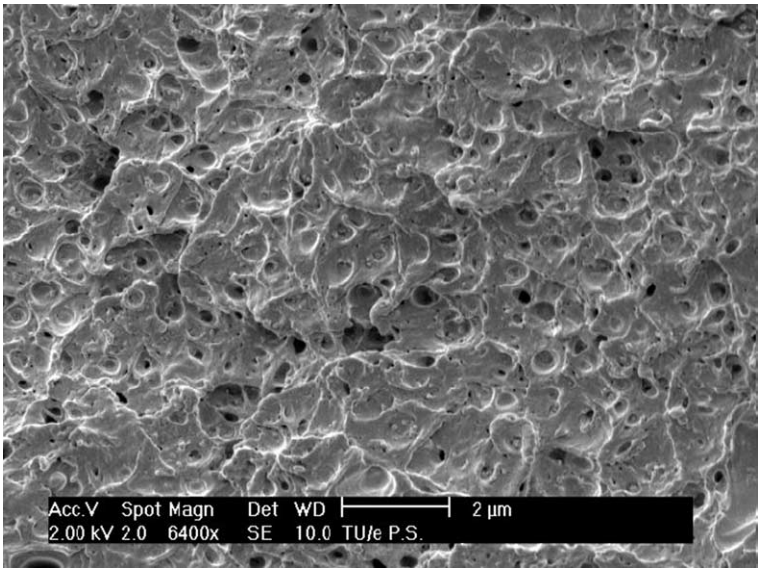

Fig. 20. SEM of the fracture surface of a PMMA matrix blended with EP(D)M-*g*-PMMA core-shell particles. The total EP(D)M content in the sample is 5%.

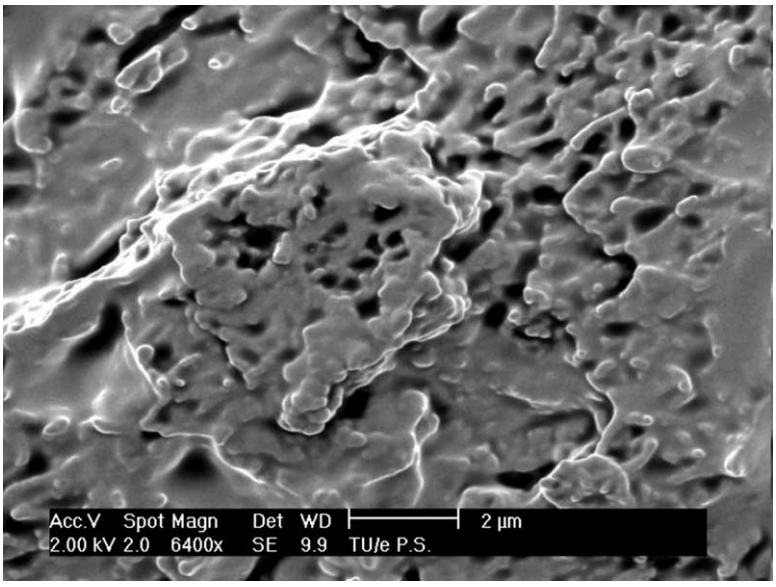

Fig. 21. SEM of the fracture surface of a PMMA matrix blended with EP(D)M-*g*-PMMA core-shell particles. The total EP(D)M content in the sample is 15%.

4. Conclusions

The present paper reports about the various morphologies that may be obtained during seeded emulsion polymerizations of MMA onto EP(D)M.

The morphology of the obtained particles was studied upon variation of several parameters, i.e. monomer type, monomer-to-EP(D)M weight ratio, monomer feed type, as well as crosslinking of the EP(D)M seed latex.

Although kinetic and thermodynamic considerations allowed the prediction of core-shell structures, there remain some discrepancies between theory and experiment. A thorough experimental investigation demonstrated that the seeded emulsion polymerization of MMA onto EP(D)M can not only result in partial engulfment of the EP(D)M seed particles by the growing PMMA chains, leading to snowman-like particles, but can also result in complete engulfment, i.e. core-shell or inverted core-shell.

In addition, it was demonstrated that EP(D)M crosslinking is a prerequisite to obtain core-shell structures. A gel content of 13% (SEP6), obtained with divinylbenzene as the only co-agent, is sufficient to limit the mobility of the EP(D)M chains and, therefore, to prevent the rubber phase from being expelled from the hard PMMA phase.

Finally, the core-shell structured particles, produced by seeded emulsion polymerization of MMA onto EP(D)M, were used to toughen a PMMA matrix. Tensile tests and scanning electron microscopy (SEM) analysis demonstrated that the main mechanism of deformation operating in the EP(D)M-toughened PMMA matrix is shear yielding, accompanied by debonding and cavitation processes. Tensile stress led to the formation of white shear bands. This stress-whitening, usually regarded as a characteristic for deformation of tough materials, symbolizes the success of our research. Finally, both SEM and TEM investigations demonstrated that the core-shell impact modifiers are more homogeneously distributed within the brittle PMMA matrix for the sample containing 5 wt% of rubbery phase. However, the tensile properties of the sample containing 15 wt% of rubber remain fairly satisfactory.

Acknowledgements

We thank Mitsui Chemicals Inc. and Crompton Corporation for the polymer samples. We are especially grateful to Paul Bomans (Maastricht University), Pauline Schmit and Anne Spoelstra for the cryo-TEM, SEM and TEM pictures, respectively. The Foundation of Emulsion Polymerization (SEP) and the European Graduate School (EGS) on 'Microstructural Control in Radical Polymerization', are gratefully acknowledged for their financial support as well as stimulating discussions.

References

[1] Mizoguchi M, Fuseya Y, Fujita Y, Ishino Y, Seki M, Miyawaki T. Patent-Eur Pat Appl 750023; 1996.
[2] Pascault J, Valette L, Magny, B. Patent-PCT Int Appl 2000059951; 2000.
[3] Tanrattanakul V, Baer E, Hiltner A, Hu R, Dimonie VL, El Aasser MS, et al. J Appl Polym Sci 1996;62:2005.
[4] El-Aasser MS, Segall I, Dimonie VL. Macromol Symp 1996;101:517.
[5] Berzinis A.P, Wills, W.L. Patent-Eur Pat Appl 265142; 1988.
[6] Troy E.J, Rosado, A. Patent-Can Pat Appl 2163941; 1996.
[7] Aerdts AM, Groeninckx G, Zirkzee HF, van Aert HAM, Geurts JM. Polymer 1997;38:4247.
[8] Lovell PA. Macromol Symp 1995;92:71.
[9] El-Aasser MS, Sudol ED. Emulsion polymerization and emulsion polymers. Chichester: Wiley; 1997. Chapter 2.
[10] Okubo M, Lu Y, Wang Z. Colloid Polym Sci 1998;276:833.

[11] Li H, Han J, Panioukhine A, Kumacheva E. J Colloid Interface Sci 2002;255:119.
[12] Tillier DL, Meuldijk J, Koning CE. Polymer 2003;44:7883.
[13] Tillier DL, Meuldijk J, Magusin PCMM, van Herk AM, Koning CE. J Polym Sci Part A: Polym Chem 2005; in press.
[14] Höhne G, Hemminger W, Flammersheim HJ. Differential scanning calorimetry. 2nd ed. Berlin: Springer; 2003. Chapter 3.
[15] Höhne GWH. Thermochim Acta 1997;304/305:209.
[16] Höhne G, Hemminger W, Flammersheim HJ. Differential scanning calorimetry. Berlin: Springer; 2003. Chapter 6.
[17] Wu S. Polymer interface and adhesion. New York: Marcel Dekker; 1982.
[18] van Krevelen DW. Properties of polymers. 3rd ed. Amsterdam: Elsevier; 1990. Chapter 8.
[19] Fowkes FM. J Phys Chem 1962;66:382.
[20] Owens DK, Wendt RC. J Appl Polym Sci 1969;13:1741.
[21] Rulison, C. Technical note No. 306 Krüss, USA; 1999.
[22] Montezinos D, Wells BG, Burns JL. J Polym Sci Polym Lett Ed 1985; 23:421.
[23] van Zyl AJP, Sanderson RD, Wet-Roos D, Klumperman B. Macromolecules 2003;36:8621.
[24] Arayapranee W, Prasassarakich P, Rempel GL. J Appl Polym Sci 2002;83:2993.
[25] Ferguson CJ, Russell GT, Gilbert RG. Polymer 2002;43:6371.
[26] Merkel MP, Dimonie VL, El Aasser MS, Vanderhoff JW. J Polym Sci Part A: Polym Chem 1987;25:1755.
[27] Merkel MP, Dimonie VL, El Aasser MS, Vanderhoff JW. J Polym Sci Part A: Polym Chem 1987;25:1219.
[28] Ferguson CJ, Russell GT, Gilbert RG. Polymer 2003;44:2607.
[29] Lee S, Rudin A. J Polym Sci Part A: Polym Chem 1992;30:865.
[30] Cho I, Lee KW. J Appl Polym Sci 1985;30:1903.
[31] Van Doremaele GHJ. PhD Thesis, University of Eindhoven; 1990.
[32] Omi S, Senba T, Nagai M, Ma GH. J Appl Polym Sci 2001;79:2200.
[33] Okubo M, Yamada A, Matsumoto T. J Polym Sci Polym Chem Ed 1980;18:3219.
[34] Torza S, Mason SG. J Colloid Interface Sci 1970;33:67.
[35] Chen YC, Dimonie V, El Aasser MS. Macromolecules 1991;24:3779.
[36] Waters JA. Colloids Surf A: Physicochem Eng Aspects 1994;83:167.
[37] Waters JA. Colloidal polymer particles. London: Academic Press Limited; 1995. Chapter 7.
[38] Sundberg DC, Casassa AP, Pantazopoulos J, Muscato MR, Kronberg B, Berg J. J Appl Polym Sci 1990;41:1425.
[39] van Zyl AJP. PhD Thesis, University of Stellenbosch; 2003.
[40] Gonzalez-Ortiz LJ, Asua JM. Macromolecules 1995;28:3135.
[41] Gonzalez-Ortiz LJ, Asua JM. Macromolecules 1996;29:383.
[42] Gonzalez-Ortiz LJ, Asua JM. Macromolecules 1996;29:4520.
[43] Mills MF, Gilbert RG, Napper DH. Macromolecules 1990;23:4247.
[44] Chern CS, Poehlein GW. J Polym Sci Part A: Polym Chem 1987;25: 617.
[45] Chern CS, Poehlein GW. J Polym Sci Part A: Polym Chem 1990;28: 3055.
[46] Chern CS, Poehlein GW. J Polym Sci Part A: Polym Chem 1990;28: 3073.
[47] Davis TP, O'Driscoll KF, Piton MC, Winnik MA. J Poly Sci Part C: Polym Lett 1989;27:181.
[48] Lide DR. CRC handbook of chemistry and physics. Boca Raton, FL: CRC; 2003.
[49] Vazquez F, Schneider M, Pith T, Lambla M. Polym Int 1996;41:1.
[50] Schneider M, Pith T, Lambla M. Polym Adv Technol 1995;6:326.
[51] Bucknall CB. Toughened plastics. London: Applied Science Publication; 1977.
[52] Lovell PA, McDonand J, Saunders DEJ, Sheratt MN, Young RJ. Adv Chem Ser 1993;233:61.
[53] Lovell PA, Pierre D. Emulsion polymerization and emulsion polymers. Chichester: Wiley; 1997. Chapter 19.
[54] Hooley CJ, Moore DR, Whale M, Williams MJ. Plast Rubber Proc Appl 1981;1:345.
[55] Bucknall CB, Partridge IK, Ward MV. J Mater Sci 1984;19:2064.
[56] Frank O, Lehmann J. Colloid Polym Sci 1986;264:473.